Supporting Information

New Reagentless Glutamate Biosensors Based on Mesophilic and Thermophilic Glutamate Dehydrogenases

Valeri Pavlov,[1] Serve Kengen,[2] Ioanis Katakis[*1]*

[1]Bioanalysis and Bioelectrochemistry Group, Chemical Engineering, Universitat Rovira i Virgili, E-43006, Tarragona (Catalonia), Spain. [2]Laboratory of Microbiology, Department of Biochemical Science, Wageningen Agricultural University, Hesselink van Suchtelenweg 4, Wageningen NL-6703 CT, Netherlands.

[*] E-mail: ioanis.katakis@urv.net. Tel: +34 977 55 9655, Fax: +34 977 55 9667.

EXPERIMENTAL SECTION

Materials. Mesophilic GLDH (E.C. 1.4.1.3) from bovine liver, as suspension in saturated ammonium sulfate was purchased from Biozyme (UK), thermophilic GLDH was purified from *Pyrococcus furiosus* as reported elsewhere.[29] Nicotinamide adenine nucleotide (NAD^+), 1,4-dihydronicotinamide adenine dinucleotide (NADH, disodium salt), alginic acid sodium salt, L-glutamic acid monosodium salt were purchased from Sigma (USA). Bromoethylamine hydrobromide, 4,4'-dimethyl-2,2'-bipyridine, sodium dihydrogen phosphate, sodium hydroxide, *ortho*-phosphoric acid, sodium chloride, thionyl chloride, NH_4PF_6, N-(3-dimethylaminopropyl)-N-ethylcarbodiimide hydrochloride were obtained from Aldrich (USA), K_2OsCl_6 - from Alfa (Spain), poly(4-vinylpyridine) (PVP) and poly(ethylene glycol) diglycedyl ether (PEGDGE) were purchased from Polysciences Inc. (USA), chloride form ion exchange beads AG 1-X8 – from BioRad Laboratories (USA). Ethylene glycol and sodium dithionite were obtained from Pancreac (Spain), Gafquat® HS100-from ISP Europe, 1,10-phenanthroline-5,6-dione was prepared by the published procedure.[34] PVP modified with amino groups was synthesized according to the procedure described elsewhere.[35]

[Os(4,4'-dimethyl-2,2'-bipyridine)$_2$Cl$_2$] and [Os(1,10-phenanthroline-5,6-dione)$_2$Cl$_2$] were synthesized according to the adapted method.[36] Generally the synthesis procedure involved refluxing of K_2OsCl_6 with 4,4'-dimethyl-2,2'-bipyridine or 1,10-phenanthroline-5,6-dione in DMF under argon in the dark for 1 hr, followed by reduction with aqueous sodium dithionite solution.

Synthesis of [Os(4,4'-dimethyl-2,2'-bipyridine)$_2$ (1,10-phenanthroline-5,6-dione)]Cl$_2$. The complex [Os(4,4'-dimethyl-2,2'-bipyridine)$_2$(1,10-phenanthroline-5,6-dione)] was synthesized according to the published procedure,[37] precipitated from a NH_4PF_6 saturated aqueous solution, ion exchanged with chloride form ion exchange beads, filtered and dried under vacuum to yield the solid product.

Synthesis of complex of Os(1,10-phenanthroline-5,6-dione)$_2$ with PVP (Os-phendione-PVP). PVP was dissolved in methanol and recrystallized twice from ether. Next 80 mg of [Os(1,10-phenanthroline-5,6-

dione)$_2$Cl$_2$] and 50 mg of PVP were mixed in 3 mL ethylene glycol. The mixture was deaerated with argon during 10 min and refluxed under argon in the dark during 1 h, the temperature of the oil bath being maintained below 220°C, next the reaction mixture was cooled to room temperature and added dropwise to 100 mL of aqueous 1 M sodium chloride solution during 15 min. The resulting mixture was left to stand over night at 4°C, the precipitate was filtered off, washed with water, and air-dried. The synthesis procedure and the structure of resulting Os-phendione-PVP are represented in Figure S-1.

Synthesis of NAD$^+$-alginate. Modification of alginic acid with NAD$^+$ was performed according to the published method.[38] 13.8 mg of sodium alginate and 70 μmol of N-(3-dimethylaminopropyl)-N-ethylcarbodiimide hydrochloride were dissolved in 15 mL of water. The pH was adjusted with aqueous HCl to 4.7 and the solution was stirred for 40 min at room temperature. Next 70 μmol of β-NAD$^+$ was added. After reajustment of pH to 4.7 the resulting solution was stirred for 12 h at room temperature. Then the reaction mixture was dialyzed against 1 L of 10 mM Tris buffer (pH 7.0) for 12 h at 4°C and then dialyzed against 1 L of water at 4°C. The dialyzate was liophylized to yield solid NAD$^+$-alginate, the structure of which can be seen in Figure S-2.

Preparation of bovine GLDH solution. In order to purify mesophilic bovine GLDH 4 mL of meso GLDH suspension in saturated ammonium sulfate solution were centrifuged during 10 min at 14000 RPM at 5°C. The precipitated enzyme was isolated from the ammonium sulfate solution and dissolved in 3 mL of 0.1 M sodium phosphate buffer (pH 7.4) containing 0.15 M sodium chloride, next the resulting enzyme solution was extensively dialyzed at 5°C against 200 ml of the same buffer during 24 h. The buffer solution was changed every two hours.

Preparation of graphite electrodes. Spectrographic graphite rods of 3 mm in diameter (Carbone of America, USA) were cut into 2 cm pieces, introduced into heat-shrinkable PVC plastic tubes, shrunk by heating, wet polished on fine (grit 400 and 600) emery paper (Buehler, USA) and sonicated in water.

Preparation of reagentless glutamate biosensors based on NAD$^+$-alginate. 1 μL of 1.8 mg/mL Os-phendione-PVP solution in ethylene glycol was deposited on a graphite electrode and left to stand for 3 min. The electrodes were washed with ethylene glycol and with water and air-dried.

a. Biosensors based on mesophilic or thermophilic GLDH. A solution containing 24 mg/mL (24 U/mL at 30°C) bovine GLDH or 1.8 mg/mL (0.7 U/mL at 40°C) GLDH from *Pyrococcus furiosus* and 28.6 mg/mL NAD$^+$-alginate in 0.1 M sodium phosphate buffer (pH 7.4) was prepared and 4 μL of the resulting mixture was placed on a Os-phendione-PVP modified electrode and dried during 1 h.

Preparation of reagentless glutamate biosensors based on crosslinked hydrogel.

a. Biosensors based on mesophilic GLDH. A solution containing 5.28 mg/mL (36 U/mL at 30°C) bovine GLDH, and 34 mg/mL NAD$^+$, 8.6 mg/mL "binder" polymer, and 1 mg/mL PEGDGE in 0.1 M sodium phosphate buffer (pH 7.4) was prepared and 4 μL of the resulting mixture was placed on a Os-phendione-PVP modified electrode and dried under vacuum during 24 h.

b. Biosensors based on thermophilic GLDH. A solution containing 3.24 mg/mL (1.2 U/mL at 40°C) bovine GLDH, and 34 mg/mL NAD$^+$, 8.6 mg/mL "binder" polymer, and 1 mg/mL PEGDGE in 0.1 M sodium phosphate buffer (pH 7.4) was prepared and 4 μL of the resulting mixture was placed on a Os-phendione-PVP modified electrode and dried under vacuum during 24 h.

Preparation of glutamate biosensors for the shelf-life stability study. Disposable screen printed electrodes, shown in Figure S-3, with a working electrode area of 1 mm^2 (KREJCI Engineering, Tisnov, Czech Republic) were employed in the shelf life study in which a number of glutamate sensors was constructed in the following way. A solution containing 5.5 U/mL thermophilic or mesophilic GLDH, 5 mM $[Os(dimethylbipyridine)_2(phendione)]Cl_2$, and 127 mg/mL NAD^+ in 0.1 M Tris buffer (pH 7.4) was prepared and 0.5 μL of the mixture were deposited on a screen printed electrode and air-dried during 5 min.

Study of glutamate biosensors in a bulk solution. A three-electrode conventional thermostabilised cell (3 mL) equipped with an $Ag/AgCl/KCl_{sat}$ reference electrode, a platinum auxiliary electrode, and a graphite electrode modified according to one of the above-mentioned methods as a working electrode. The buffer, pH 7.4 (0.1 M sodium phosphate containing 0.15 M sodium chloride) served as supporting electrolyte. The response to successive additions of stock glutamate solution was registered as steady state current on a three-electrode potentiostat Autolab PGSTAT 10 (Eco chemie, Holland) controlled by a computer. The working potential was 150 mV *vs.* $Ag/AgCl/KCl_{sat}$ and the temperature of the thoroughly stirred solution was 30° or 40°C.

Shelf-life study of glutamate biosensors. Disposable glutamate biosensors were connected to the potentiostat Autolab PGSTAT 10 in the following way: the carbon electrode was connected to the working lead and Ag/AgCl reference electrode to the reference and auxiliary leads, next the biosensor was fixed during 5 min on a glass heat exchanger thermostabilized at 40°C. In order to determine the response of the sensor 0.5 μL of a sample solution was deposited and after 20 s a potential of 200 mV *vs.* Ag/AgCl electrode was applied to the working electrode. The current after 30 s (starting from the moment of applying the potential) was recorded for every electrode. Between three and five sensors were used for measurements at every point. All sensors were assayed by depositing three different samples: 0.1 M Tris buffer, pH 7.4 (containing 0.15 M NaCl), or 0.6 M glutamate solution in this buffer, or 0.6 M glutamate solution with 0.18 M NAD^+ in the buffer.

GLDH assay method. Both mesophilic and thermophilic GLDH were tested spectrophotometrically by following the increase in absorbance at 340 nm at 30°C or 40°C. The assay solution contained 5 mM NAD^+ and 10 mM in 0.1 M sodium phosphate buffer (pH 7.4). The ΔA_{340} (Au/min) was obtained using the maximum linear rate for both the test and blank (without enzyme) mixtures. The activity was calculated using ε_{NADH} = 6.22 $mM^{-1}cm^{-1}$ extinction coefficient of β-NADH. One unit of GLDH oxidizes 1 μmol of L-glutamate per minute at pH 7.4 at 30 or 40°C. Protein concentration was determined spectrophotometrically at A_{280} using an absorbance coefficient of 0.973 cm^2/mg.

Electrochemical conversion experiment. To determine the amount of enzymatically active NAD^+ produced, during the bulk electrolysis, by the oxidation of NADH at the surface of graphite electrode modified with NADH oxidizing polymer Os-phendione-PVP the electrochemical conversion experiment has been carried out in argon-saturated solution as follows. A graphite electrode (6 mm in diameter) was produced by the above-mentioned method and 4 μl of 1.8 mg/ml Os-phendione-PVP solution in ethylene glycol were deposited on its surface and left for 3 min. The electrode was washed with ethylene glycol and water. Then it was inserted into 2 ml of 18.97 μM NADH solution in 0.1 M phosphate buffer containing 0.15 M sodium chloride (pH 7.4) and poised at 150 mV vs. $Ag/AgCl/KCl_{sat}$ in a three electrode electrochemical cell at room temperature. NADH absorbance at 340

nm was followed during 7 h until it had declined to 10% of the initial value to give the resulting solution, which was used as a coenzyme for glutamate dehydrogenase. The rate of NADH reduction was monitored by change in A_{340} till the constant value. The values of A_{340} were compared with those for controlled NADH solution which had been saturated with argon without electrolysis during the time of the conversion experiment to take into account the spontaneous hydrolysis of NADH.

STEADY-STATE KINETIC MODEL OF BIOSENSORS

Figure S-4 illustrates the kinetic scheme for the operation of reagentless biosensors based on glutamate dehydrogenase enzyme (E) catalyzing the reaction of immobilized NAD^+ (A) with a L-glutamate (B) to give immobilized NADH (P), α–ketoglutarate (Q), and NH_4^+ (R). The mediator (M), which can stay in reduced (M_{red}) and oxidized (M_{ox}) forms, immobilized on the electrode surface catalyzes the electrochemical conversion of P back to A. A_{im} and P_{im} are the concentrations of immobilized A and P. B_o, Q_o, R_o are the concentrations of the substrate and the products in the hydrogel. B_∞, Q_∞ and R_∞ are the concentrations of the substrate and the products in the external medium. k'_B, k'_Q and k'_R are mass transfer constants of the substrate and the products (cm s^{-1}), respectively. L is the thickness of the hydrogel layer. The following expressions for the flux of P_{im} to the electrode surface (j_{el}), which determines the current density of a biosensor (j) through the equation $j = nFj_{el}$, where n is the number of exchanged electrons and F is the Faraday's constant (96487 C/mol), can be obtained.

$$j_{el} = k'_B(B_\infty - B_o) \quad \text{(S-1)}$$
$$j_{el} = L(k_1 A_{im}[E] - k_{-1}[E\cdot A]) \quad \text{(S-2)}$$
$$j_{el} = L(k_2 B_o[E\cdot A] - k_{-2}[E\cdot A\cdot B]) \quad \text{(S-3)}$$
$$j_{el} = L(k_3 [E\cdot A\cdot B] - k_{-3}[E\cdot P\cdot Q\cdot R]) \quad \text{(S-4)}$$
$$j_{el} = L(k_4 [E\cdot P\cdot Q\cdot R] - k_{-4}[E\cdot P\cdot Q]Q_o) \quad \text{(S-5)}$$
$$j_{el} = L(k_5 [E\cdot P\cdot Q] - k_{-5}[E\cdot P]Q_o) \quad \text{(S-6)}$$
$$j_{el} = L(k_6 [E\cdot P] - k_{-6}[E]P_{im}) \quad \text{(S-7)}$$
$$j_{el} = k'_Q Q_o \quad \text{(S-8)}$$
$$j_{el} = k'_R R_o \quad \text{(S-9)}$$
$$j_{el} = k_7 P_o \Gamma_{Mox} - k_{-7}\Gamma_{M\cdot P} \quad \text{(S-10)}$$
$$j_{el} = k_8 \Gamma_{M\cdot P} \quad \text{(S-11)}$$
$$j_{el} = k_S \Gamma_{Mred} \quad \text{(S-12)}$$
$$E_t = [E] + [E\cdot A] + [E\cdot A\cdot B] + [E\cdot P\cdot Q\cdot R] + [E\cdot P\cdot Q] + [E\cdot P] \quad \text{(S-13)}$$
$$\Gamma = \Gamma_{M\cdot P} + \Gamma_{Mox} + \Gamma_{Mred} \quad \text{(S-14)}$$
$$A_t = A_{im} + P_{im} \quad \text{(S-15)}$$

Where Γ_{Mox} and Γ_{Mred} are surface coverages of the mediator in oxidized and reduced forms, respectively. Γ is the total mediator surface coverage. $\Gamma_{M\cdot P}$ is the surface coverage of the intermediate complex between the mediator and NADH. A_t and E_t are the total concentrations of NAD^+ and the enzyme immobilized in the hydrogel, respectively. k_1, k_2, … k_6 are the rate constants of the elemental enzymatic reactions in forward direction. k_{-1}, k_{-2}, … k_{-6} are the rate constants of the elemental enzymatic reactions in backward direction. k_7 is the rate constant of the reaction between NADH oxidizing mediator and NADH, k_{-7} is the rate constant of the decomposition of the mediator-NADH complex into NADH and the oxidized mediator, k_8 is the rate constant of

the decomposition of mediator-NADH complex into the reduced mediator and NAD^+. k_S the the heterogeneous electron transfer rate constant. The equations (S-2 - S7, S-13) yield the equation (S-16) describing the enzyme kinetics

$$j_{el} = \frac{E_t L(k_1k_2k_3k_4k_5k_6 A_{im}B_o - k_{-1}k_{-2}k_{-3}k_{-4}k_{-5}k_{-6}P_{im}Q_oR_o)}{\begin{aligned}&k_5k_6k_{-1}k_{-2}k_{-3} + k_4k_5k_6k_{-1}k_{-2} + k_{-1}k_3\ k_4k_5\ k_6 + (k_1k_5k_6k_{-2}k_{-3} + k_1k_4k_5k_6k_{-2} + k_1k_3k_4k_5k_6)A_{im} + \\ &k_2k_3k_4k_5k_6B_o + (k_1k_2k_5k_6k_{-3} + k_1k_2k_4k_5k_6 + k_1k_2k_3k_5k_6 + k_1k_2k_3k_4k_6 + k_1k_2k_3k_4k_5)A_{im}B_o + \\ &(k_5k_{-1}k_{-2}k_{-3}k_{-6} + k_4k_5k_{-1}k_{-2}k_{-6} + k_3k_4k_5k_{-1}k_{-6})P_{im} + k_6k_{-1}k_{-2}k_{-3}k_{-4}R_o + k_{-1}k_{-2}k_{-3}k_{-4}k_{-5}R_oQ_o + \\ &(k_{-1}k_{-2}k_{-3}k_{-5}k_{-6} + k_4k_{-1}k_{-2}k_{-5}k_{-6} + k_3k_4k_{-1}k_{-5}k_{-6})P_{im}Q_o + (k_{-2}k_{-3}k_{-4}k_{-5}k_{-6} + k_{-1}k_{-3}k_{-4}k_{-5}k_{-6} + \\ &k_{-1}k_{-2}k_{-4}k_{-5}k_{-6} + k_3k_{-1}k_{-4}k_{-5}k_{-6})P_{im}Q_oR_o + k_{-1}k_{-2}k_{-3}k_{-4}k_{-6}P_{im}R_o + k_2k_3k_4k_5k_{-6}B_oP_{im} + \\ &k_2k_3k_4k_{-5}k_{-6}B_oP_{im}Q_o + k_1k_2k_3k_4k_{-5}A_{im}B_oQ_o + k_1k_{-2}k_{-3}k_{-4}k_{-5}A_{im}R_oQ_o + k_1k_6k_{-2}k_{-3}k_{-4}A_{im}R_o + \\ &(k_1k_2k_{-3}k_{-4}k_{-5} + k_1k_2k_3k_{-4}k_{-5})\,A_{im}B_oR_oQ_o + (k_2k_{-3}k_{-4}k_{-5}k_{-6} + k_2k_3k_{-4}k_{-5}k_{-6})\,B_oR_oP_{im}Q_o + \\ &(k_1k_2k_6k_{-3}k_{-4} + k_1k_2k_3k_6k_{-4})\,A_{im}B_oR_o\end{aligned}}$$

(S-16)

When numerator and denominator of this rate equation are multiplied by the factor $(k_{-1}k_{-2}k_{-3}k_{-4}k_{-5}k_{-6})/((k_1k_2k_5k_6k_{-3} + k_1k_2k_4k_5k_6 + k_1k_2k_3k_5k_6 + k_1k_2k_3k_4k_6 + k_1k_2k_3k_4k_5)(k_{-2}k_{-3}k_{-4}k_{-5}k_{-6} + k_{-1}k_{-3}k_{-4}k_{-5}k_{-6} + k_{-1}k_{-2}k_{-4}k_{-5}k_{-6} + k_3k_{-1}k_{-4}k_{-5}k_{-6}))$ the equation S-17 can be obtained:

$$j_{el} = \frac{L(V_1V_2A_{im}B_o - (V_1V_2P_{im}Q_oR_o)/K_{eq})}{\begin{aligned}&K_{AB}V_2 + K_BV_2A_{im} + K_AV_2B_o + V_2A_{im}B_o + K_{QR}V_1P_{im}/K_{eq} + K_{PQ}V_1R_o/K_{eq} + K_PV_1Q_oR_o/K_{eq} + \\ &K_RV_1P_{im}Q_o/K_{eq} + V_1P_{im}Q_oR_o/K_{eq} + K_QV_1R_oP_{im}/K_{eq} + K_AV_2B_oP_{im}/K_{iP} + K_AV_2B_oP_{im}Q_o/(K_{iQ}K_{iP}) + \\ &K_{iR}K_PV_1A_{im}B_oQ_o/(K_{iA}K_{iB}K_{eq}) + K_PV_1A_{im}R_oQ_o/(K_{iA}K_{eq}) + K_{PQ}V_1A_{im}R_o/(K_{iA}K_{eq}) + \\ &K_PV_1A_{im}B_oQ_oR_o/(K_{iA}K_{iB}K_{eq}) + K_AV_2B_oR_oP_{im}Q_o/(K_{iR}K_{iP}K_{iQ}) + K_{PQ}V_1A_{im}B_oR_o/(K_{iA}K_{iB}K_{eq})\end{aligned}}$$

(S-17)

Where $V_1 = E_t(k_1k_2k_3k_4k_5k_6)/(k_1k_2k_5k_6k_{-3} + k_1k_2k_4k_5k_6 + k_1k_2k_3k_5k_6 + k_1k_2k_3k_4k_6 + k_1k_2k_3k_4k_5)$ and $V_2 = E_t(k_{-1}k_{-2}k_{-3}k_{-4}k_{-5}k_{-6})/(k_{-2}k_{-3}k_{-4}k_{-5}k_{-6} + k_{-1}k_{-3}k_{-4}k_{-5}k_{-6} + k_{-1}k_{-2}k_{-4}k_{-5}k_{-6} + k_3k_{-1}k_{-4}k_{-5}k_{-6})$ are the maximum velocities in forward and reverse directions, the equilibrium constant $K_{eq}=k_1k_2k_3k_4k_5k_6/(k_{-1}k_{-2}k_{-3}k_{-4}k_{-5}k_{-6})$, the Michaelis constants for A, B, P, Q, R are $K_A = (k_2k_3k_4k_5k_6)/(k_1k_2k_5k_6k_{-3} + k_1k_2k_4k_5k_6 + k_1k_2k_3k_5k_6 + k_1k_2k_3k_4k_6 + k_1k_2k_3k_4k_5)$, $K_B = (k_1k_5k_6k_{-2}k_{-3} + k_1k_4k_5k_6k_{-2} + k_1k_3k_4k_5k_6)/(k_1k_2k_5k_6k_{-3} + k_1k_2k_4k_5k_6 + k_1k_2k_3k_5k_6 + k_1k_2k_3k_4k_6 + k_1k_2k_3k_4k_5)$, $K_{AB} = (k_5k_6k_{-1}k_{-2}k_{-3} + k_4k_5k_6k_{-1}k_{-2} + k_{-1}k_3\ k_4k_5\ k_6)/(k_1k_2k_5k_6k_{-3} + k_1k_2k_4k_5k_6 + k_1k_2k_3k_5k_6 + k_1k_2k_3k_4k_6 + k_1k_2k_3k_4k_5)$, $K_P = k_{-1}k_{-2}k_{-3}k_{-4}k_{-5}/(k_{-2}k_{-3}k_{-4}k_{-5}k_{-6} + k_{-1}k_{-3}k_{-4}k_{-5}k_{-6} + k_{-1}k_{-2}k_{-4}k_{-5}k_{-6} + k_3k_{-1}k_{-4}k_{-5}k_{-6})$, $K_Q = k_{-1}k_{-2}k_{-3}k_{-4}k_{-6}/(k_{-2}k_{-3}k_{-4}k_{-5}k_{-6} + k_{-1}k_{-3}k_{-4}k_{-5}k_{-6} + k_{-1}k_{-2}k_{-4}k_{-5}k_{-6} + k_3k_{-1}k_{-4}k_{-5}k_{-6})$, $K_R = (k_{-1}k_{-2}k_{-3}k_{-5}k_{-6} + k_4k_{-1}k_{-2}k_{-5}k_{-6} + k_3k_4k_{-1}k_{-5}k_{-6})/(k_{-2}k_{-3}k_{-4}k_{-5}k_{-6} + k_{-1}k_{-3}k_{-4}k_{-5}k_{-6} + k_{-1}k_{-2}k_{-4}k_{-5}k_{-6} + k_3k_{-1}k_{-4}k_{-5}k_{-6})$, $K_{QR} = (k_5k_{-1}k_{-2}k_{-3}k_{-6} + k_4k_5k_{-1}k_{-2}k_{-6} + k_3k_4k_5k_{-1}k_{-6})/(k_{-2}k_{-3}k_{-4}k_{-5}k_{-6} + k_{-1}k_{-3}k_{-4}k_{-5}k_{-6} + k_{-1}k_{-2}k_{-4}k_{-5}k_{-6} + k_3k_{-1}k_{-4}k_{-5}k_{-6})$, $K_{PQ} = k_6k_{-1}k_{-2}k_{-3}k_{-4}/(k_{-2}k_{-3}k_{-4}k_{-5}k_{-6} + k_{-1}k_{-3}k_{-4}k_{-5}k_{-6} + k_{-1}k_{-2}k_{-4}k_{-5}k_{-6} + k_3k_{-1}k_{-4}k_{-5}k_{-6})$.

The inhibition constants for A, B, P, Q, R are $K_{iA} = k_{-1}/k_1$, $K_{iB} = (k_{-2}k_{-3})/(k_2(k_{-3} + k_3))$, $K_{iP} = k_6/k_{-6}$, $K_{iQ} = k_5/k_{-5}$, $K_{iR} = (k_3k_4)/(k_{-4}(k_3 + k_{-3}))$. Using the inhibition constants allows to redefine: $K_{PQ}=K_{iP}K_Q$ and $K_{QR}=K_{iQ}K_R$.

After division of the numerator and the denominator in the equation S-17 by V_2 and substitution of $V_1/(V_2K_{eq})$ with $(K_BK_{iA})/(K_{iQ}K_{iP}K_R)$ one can obtain the equation:

$$j_{el} = \frac{L(V_1A_{im}B_o - (V_1P_{im}Q_oR_o)/K_{eq})}{\begin{array}{l}K_{AB} + K_BA_{im} + K_AB_o + A_{im}B_o + K_{QR}K_{iA}K_BP_{im}/(K_{iP}K_{iQ}K_R) + K_{PQ}K_{iA}K_BR_o/(K_{iP}K_{iQ}K_R) + \\ K_PK_{iA}K_BQ_oR_o/(K_{iP}K_{iQ}K_R) + K_RK_{iA}K_BP_{im}Q_o/(K_{iP}K_{iQ}K_R) + K_{iA}K_BP_{im}Q_oR_o/(K_{iP}K_{iQ}K_R) + \\ K_PK_{iA}K_BR_oP_{im}/(K_{iP}K_{iQ}K_R) + K_AB_oP_{im}/K_{iP} + K_AB_oP_{im}Q_o/(K_{iQ}K_{iP}) + \\ K_{iR}K_PK_BA_{im}B_oQ_o/(K_{iB}K_{iP}K_{iQ}K_R) + K_PK_BA_{im}R_oQ_o/(K_{iP}K_{iQ}K_R) + K_{PQ}K_BA_{im}R_o/(K_{iP}K_{iQ}K_R) + \\ K_PK_B\,A_{im}B_oQ_oR_o/(K_{iB}K_{iP}K_{iQ}K_R) + K_AB_oR_oP_{im}Q_o/(K_{iR}K_{iP}K_{iQ}) + K_{PQ}K_BA_{im}B_oR_o/(K_{iB}K_{iP}K_{iQ}K_R)\end{array}}$$

(S-18)

The equations (S-10 – S-12, S-14) give the equation (S-19) which governs the kinetics of NADH oxidation at the electrode surface modified with a mediator

$$j_{el} = \frac{\Gamma k_7k_8k_SP_o}{k_8k_S + k_{-7}k_S + (k_7k_8 + k_7k_S)P_{im}} = \frac{\Gamma P_{im}\,k_7k_8k_S/(k_7k_8 + k_7k_S)}{(k_8k_S + k_{-7}k_S)/(k_7k_8 + k_7k_S) + P_{im}} = \frac{k_{cat}\Gamma P_{im}}{k_M + P_{im}}$$

(S-19)

where the Michaelis constant for the mediator M is $k_M = (k_8k_S + k_{-7}k_S)/(k_7k_8 + k_7k_S)$ and $k_{cat} = k_8k_S/(k_8 + k_S)$. Using the equations (S-15) and (S-19) the concentrations of NAD^+ and NADH (A_{im} and P_{im}) as well as B_o, Q_o and R_o from (S-1), (S-8) and (S-9) can be found: $P_{im} = j_{el}K_M/(k_{cat}\Gamma_M - j_{el})$, $A_{im} = A_t - P_{im} = A_t - j_{el}K_M/(k_{cat}\Gamma_M - j_{el})$, $B_o = B_\infty - j_{el}/k'_B$, $Q_o = j_{el}/k'_Q$, $R_o = j_{el}/k'_R$. Substitution of A_{im}, B_o, P_{im}, Q_o, R_o into the equation (S-18) with their expressions gives the following equation of the fourth order:

$$\begin{array}{l}LV_1\Gamma k_{cat}E_tA_tB_\infty = j_{el}[K_{AB}\Gamma k_{cat} + K_B\Gamma k_{cat}A_t + K_A\Gamma k_{cat}B_\infty + A_t\Gamma k_{cat}B_\infty + LV_1(A_t + K_M)B_\infty + (LV_1A_t\Gamma k_{cat})/k'_B] + \\ j^2_{el}[(K_{PQ}K_BA_t\Gamma k_{cat})/(K_{iP}K_{iQ}K_Rk'_R) - LV_1(A_t + K_M)/k'_B - K_{AB} - K_B(A_t + K_M) - K_AB_\infty + K_MK_{QR}K_{iA}K_B/(K_{iP}K_{iQ}K_R) - \\ (A_t + K_M)B_\infty - A_t\Gamma k_{cat}/k'_B + \Gamma k_{cat}K_{PQ}K_{iA}K_BR_o/(K_{iP}K_{iQ}K_Rk'_R) + K_AK_MB_\infty/K_{iP} + K_{iR}K_PK_BA_tB_\infty\Gamma k_{cat}/(K_{iB}K_{iP}K_{iQ}K_Rk'_Q) + \\ K_{PQ}K_BA_tB_\infty\Gamma k_{cat}/(K_{iB}K_{iP}K_{iQ}k'_R)] + J^3_{el}[LV_1K_M/(K_{eq}k'_Qk'_R) + K_A/k'_B + (A_t + K_M)/k'_B - K_{PQ}K_{iA}K_B/(K_{iP}K_{iQ}K_Rk'_R) + \\ \Gamma k_{cat}K_PK_{iA}K_B/(K_{iP}K_{iQ}K_R\,k'_Qk'_R) + K_MK_RK_{iA}K_B/(K_{iP}K_{iQ}K_Rk'_Q) + K_MK_PK_{iA}K_B/(K_{iP}K_{iQ}K_Rk'_R) - K_AK_M/(K_{iP}k'_B) + \\ K_AK_MB_\infty/(K_{iQ}K_{iP}k'_Q) - K_{iR}K_PK_B(A_t + K_M)B_\infty/(K_{iB}K_{iP}K_{iQ}K_Rk'_Q) - K_{iR}K_PK_BA_t\Gamma k_{cat}/(K_{iB}K_{iP}K_{iQ}K_R\,k'_Bk'_Q) + \\ K_PK_BA_t\Gamma k_{cat}/(K_{iP}K_{iQ}K_Rk'_Qk'_R) - K_{PQ}K_B(A_t + K_M)/(K_{iP}K_{iQ}K_Rk'_R) + K_PK_BA_tB_\infty\Gamma k_{cat}/(K_{iB}K_{iP}K_{iQ}K_Rk'_Qk'_R) - \\ K_{PQ}K_BB_\infty(A_t + K_M)/(K_{iB}K_{iP}K_{iQ}K_Rk'_R) - A_t\Gamma k_{cat}K_{PQ}K_B/(K_{iB}K_{iP}K_{iQ}K_Rk'_Bk'_R)] + J^4_{el}[K_{iA}K_BK_M/(K_{iP}K_{iQ}K_Rk'_Qk'_R) - \\ K_PK_{iA}K_B/(K_{iP}K_{iQ}K_Rk'_Qk'_R) - K_AK_M/(K_{iQ}K_{iP}k'_Bk'_Q) + K_{iR}K_PK_B(A_t + K_M)/(K_{iB}K_{iP}K_{iQ}K_Rk'_Bk'_Q) - \\ K_PK_B(A_t + K_M)/(K_{iP}K_{iQ}K_Rk'_Qk'_R) - K_PK_BB_\infty/(K_{iB}K_{iP}K_{iQ}K_Rk'_Qk'_R) - K_PK_BA_t\Gamma k_{cat}/(K_{iB}K_{iP}K_{iQ}K_Rk'_Bk'_Qk'_R) + \\ K_AB_\infty K_M/(K_{iR}K_{iP}K_{iQ}k'_Qk'_R) + K_{PQ}K_B(A_t + K_M)/(K_{iB}K_{iP}K_{iQ}K_Rk'_Bk'_R)] + j^5_{el}[K_PK_B(A_t + K_M)/(K_{iB}K_{iP}K_{iQ}K_Rk'_Bk'_Qk'_R) \\ - K_AK_M/(K_{iR}K_{iP}K_{iQ}k'_Bk'_Qk'_R)]\end{array}$$

(S-20)

The equation S-20 was employed to simulate the response curves and Eadie-Hofstee plots for the reagentless glutamate biosensors using the values of the Michaelis constants and inhibition constants from the literature.[53] Figure S-5 shows the effect of NAD^+ loading on the response to glutamate of biosensors which are not limited neither by Os-phendione-PVP loading nor by the mass transport. The Eadie-Hofstee plots show straight lines which are characteristic for the process of enzymatic oxidation of glutamate limited only the concentration of NAD^+. At saturating NAD^+ loading the values of the apparent maximum current density and the apparent

Michaelis constant coincide with those of the product LV_1nF and the Michaelis constant (K_B) respectively. The decrease in the NAD^+ loading results in the decrease in the values of slopes and intercepts of Eadie-Hofstee plots with the axis of j, which are the apparent Michaelis constants for the substrate B and the maximum current densities respectively.

Figure S-6 demonstrates the effect of the rate of mass transport of the substrate and reaction products on the response of glutamate electrodes. The simulation of the response to glutamate was performed using saturating loading of NAD^+ ($A_t \rightarrow \infty$) and the infinitively high maximum flux of the electrochemical oxidation of NADH ($\Gamma k_{cat} \rightarrow \infty$). The decrease in the mass transfer constants results in more convex shape of the Eadie-Hofstee plots leading to the decrease in the values of intercepts of the Eadie-Hofstee plots with the axis of j i.e. the apparent maximum current densities become lower due to the accumulation of the reaction products Q and R in the hydrogel leading to the inhibition of the reaction of glutamate oxidation. The values of apparent maximum current densities coincide with the value of LV_1nF only when the rate of mass transport is infinitively high resulting in infinitively low steady state concentrations of reaction products Q and R in the hydrogel. This means that the convex Eadie-Hofstee plots are diagnostic for the glutamate electrodes limited by rate of mass transfer.

The effect of the value of the maximum flux of the electrochemical oxidation of NADH (Γk_{cat}) on the simulated response of reagentless glutamate biosensors (at A_t = 1 mM) is demonstrated in Figure S-7. The Eadie-Hofstee plots give the straight line characteristic for the process limited by the enzymatic reduction of NAD^+ only when Γk_{cat} is infinitively high. The decrease in the value of Γk_{cat} leads to the decrease in the values of intercepts of the Eadie-Hofstee plots with the axis of j and their slopes i.e. the apparent maximum current densities and apparent Michaelis constants become lower due to the limitation set by the flux of the electrochemical oxidation of NADH (Table S-I). The decrease in the value of Γk_{cat} also affects the shape of the Eadie-Hofstee plots making them more concave. Hence, the concavity of Eadie-Hofstee plots is diagnostic for reagentless glutamate biosensors limited by the rate of electrochemical NADH oxidation at the electrode surface.

Figure S-8 represents the effect of mass transport rate on the response of biosensors limited by the rate of the electrochemical NADH oxidation. The decrease in the mass transfer constants leads to the drastic increase in the slope of the Eadie-Hofstee plots, making the apparent Michaelis constants (measured using high concentrations of glutamate) even higher than K_B of free GLDH (Table S-II). It can be concluded that the concave Eadie-Hofstee plots, giving the values of the apparent Michaelis constant higher than the value of K_M of the free enzyme, are diagnostic for reagentless glutamate biosensors limited by the rate of electrochemical NADH oxidation at the electrode surface and by the rate of mass transport.

The effect of the maximum flux of the enzymatic reduction of NAD^+ (LV_1) rate on the response of biosensors limited by the rate of the electrochemical NADH oxidation and mass transport is demonstrated in Figure S-9. The increase in LV_1 leads to the drastic increase in apparent current densities and the concavity of Eadie-Hofstee plots, making the apparent Michaelis constants higher than K_B of free GLDH (Table S-III).

GLOSSARY

A_t	total cofactor concentration in the hydrogel (M)
A_{im}	concentration of NAD^+ immobilized in the hydrogel (M)
B_o	substrate concentration in the hydrogel (M)
B_∞	substrate concentration in the external medium (M)
E_t	total enzyme concentration (M)
F	Faraday's constant (96487 C mol^{-1})
GLDH	glutamate dehydrogenase
j_{el}	flux of reactants (mol cm^{-2} s^{-1})
j	current density (A cm^{-2})
k	rate coefficient of the formal overall chemical reaction of NADH oxidation by the mediator (M^{-1} s^{-1})
$k_{[NADH]=0}$	rate coefficient of the formal overall chemical reaction of NADH oxidation by the mediator extrapolated to zero concentration of NADH (M^{-1} s^{-1})
k_S	heterogeneous electron transfer rate constant (s^{-1})
k_7	rate constant of the reaction between the NADH oxidizing mediator and NADH ($M^{-1}s^{-1}$)
k_{-7}	rate constant of the decomposition of the mediator-NADH complex into NADH and the oxidized mediator (s^{-1})
k_8	the rate constant of the decomposition of mediator-NADH complex into the reduced mediator and NAD^+ (s^{-1})
k_1, k_2, k_3, k_4, k_5, k_6	rate constants of the elemental enzymatic reactions in forward direction (M^{-1} s^{-1}, M^{-1} s^{-1}, s^{-1}, s^{-1}, s^{-1}, s^{-1} respectively)
k_{-1}, k_{-2}, k_{-3}, k_{-4}, k_{-5}, k_{-6}	rate constants of the elemental enzymatic reactions in reverse direction (s^{-1}, s^{-1}, s^{-1}, s^{-1}, M^{-1} s^{-1}, M^{-1} s^{-1} respectively)
k'_B	mass transfer rate coefficient for the substrate B (cm s^{-1})
k'_Q	mass transfer rate coefficient for the product Q (cm s^{-1})
k'_R	mass transfer rate coefficient for the product R (cm s^{-1})
K_M	Michaelis constant of Os-phendione-PVP (M)
L	thickness of the hydrogel layer (cm)
n	number of exchanged electrons
P_{im}	concentration of NADH immobilized in the hydrogel (M)
PVP	poly(4-vinyl pyridine)
phendione	1,10-phenanthroline-5,6-dione
R_∞	concentration of product R in the external medium (M)

R_o	concentration of product R in the hydrogel (M)
V_1	maximum velocity of the enzymatic reaction in forward direction (s^{-1})
V_2	maximum velocity of the enzymatic reaction in reverse direction (s^{-1})
Q_∞	concentration of product Q in the external medium (M)
Q_o	concentration of product Q in the hydrogel (M)

Greek letters

Γ	total surface coverage of Os-phendione-PVP (mol cm^{-2})
Γ_{Mox}	surface coverage of the mediator in the oxidized form (mol cm^{-2})
Γ_{Mred}	surface coverage of the mediator in the reduced form (mol cm^{-2})
$\Gamma_{M \cdot P}$	surface coverage of the intermediate complex between Os-phendione-PVP and NADH (mol cm^{-2})
ω	rotation speed (rad s^{-1})

TABLES AND TABLE LEGENDS

Table S-I. Effect of maximum flux of the electrochemical NADH oxidation on apparent Michaelis constants and maximum current densities given by simulated Eadie-Hofstee plots in the range of high glutamate concentrations. The values of parameters used in the simulation are the same as in Figure S-7.

Γk_{cat}, mol s^{-1} cm^{-2}	2.6×10^{-11}	1.04×10^{-10}	4.15×10^{-10}	8.3×10^{-10}	1.7×10^{-9}	1.3×10^{-8}	5.18×10^{-8}	∞
$j_{max\ app}$, μA cm^{-2}	0.927	2.055	4.195	5.923	8.270	20.37	33.06	56.91
$K_{B\ app}$, mM	0.89	1.18	1.2	1.23	1.28	1.43	1.67	2.25

Table S-II. Effect of mass transfer constants on the apparent Michaelis constants and maximum current densities given by simulated Eadie-Hofstee plots in the range of high glutamate concentrations. The values of parameters used in the simulation are the same as in Figure S-8.

k'_B, k'_Q, k'_R, cm s^{-1}	5.18×10^{-12}	2.60×10^{-11}	5.18×10^{-11}	1.03×10^{-10}	2.6×10^{-10}	∞
$j_{max\ app}$, μA cm^{-2}	5.260	5.422	5.881	5.893	5.921	5.923
$K_{B\ app}$, mM	99.4	8.80	3.60	1.99	1.42	1.24

Table S-III. Effect of the maximum flux of the enzymatic reduction of NAD^+ (LV_1) on apparent Michaelis constants and maximum current densities given by simulated Eadie-Hofstee plots in the range of high glutamate concentrations. The values of parameters used in the simulation are the same as in Figure S-9.

LV_1, Mol s^{-1} cm^{-2}	1.55×10^{-10}	3.63×10^{-10}	6.22×10^{-10}	1.24×10^{-9}	2.49×10^{-9}
$j_{max\ app}$, μA cm^{-2}	3.772	5.837	7.631	10.64	14.39
$K_{B\ app}$, mM	3.87	9.11	18.6	45.5	92.8

Table S-IV. Results of shelf life study of glutamate biosensors.

Composition of enzyme solution used for modification of screen printed electrodes	Half shelf life, h
Mesophilic GLDH (11 U/mL)	7
Thermophilic GLDH (11 U/mL)	75
Mesophilic GLDH (11 U/mL) with Gafquat® HS100 (0.0482 % w/v)	32
Thermophilic GLDH (11 U/mL) and poly(ethylene imine) (0.24% w/v)	38
Mesophilic GLDH (11 U/mL) with glycerol (20 % w/v)	6<
Thermophilic GLDH (11 U/mL) with glycerol (20 % w/v)	6<
Mesophilic GLDH (11 U/mL) with Gafquat® HS100 (0.0482 % w/v) and glycerol (20 % w/v)	6<
Thermophilic GLDH (11 U/mL) with poly(ethylene imine) (0.24% w/v) and glycerol (20 % w/v)	6<
Thermophilic GLDH (11 U/mL) with Gafquat® HS100 (0.946 % w/v)	246
Thermophilic GLDH (11 U/mL) with trehalose (14 % w/v)	80
Mesophilic GLDH (11 U/mL) with trehalose (0.85 % w/v)	8

FIGURES AND FIGURE LEGENDS

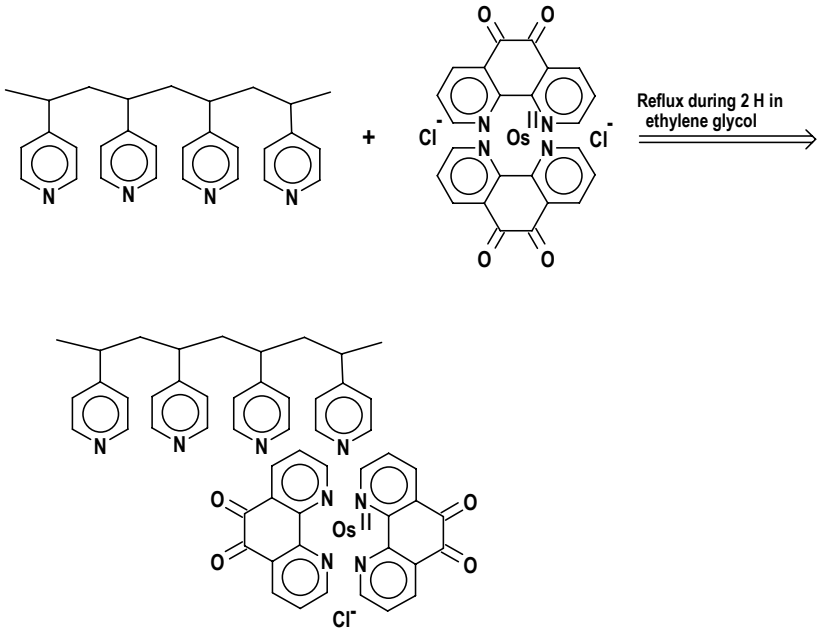

Figure S-1. Synthetic route to NADH oxidizing polymer Os-phendione-PVP.

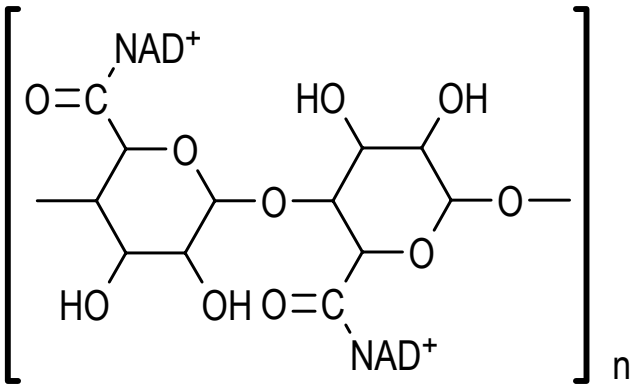

Figure S-2. Structure of NAD^+-alginate.

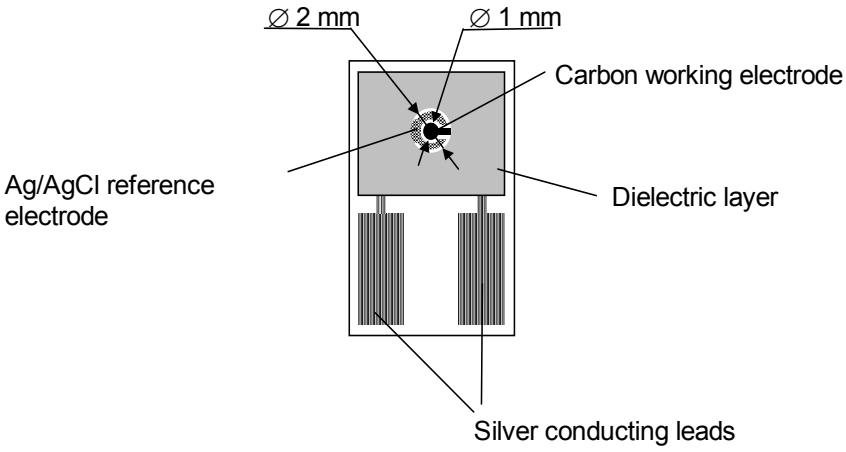

Figure S-3. Sketch of a screen printed disposable electrode utilized in the shelf stability study of glutamate biosensors.

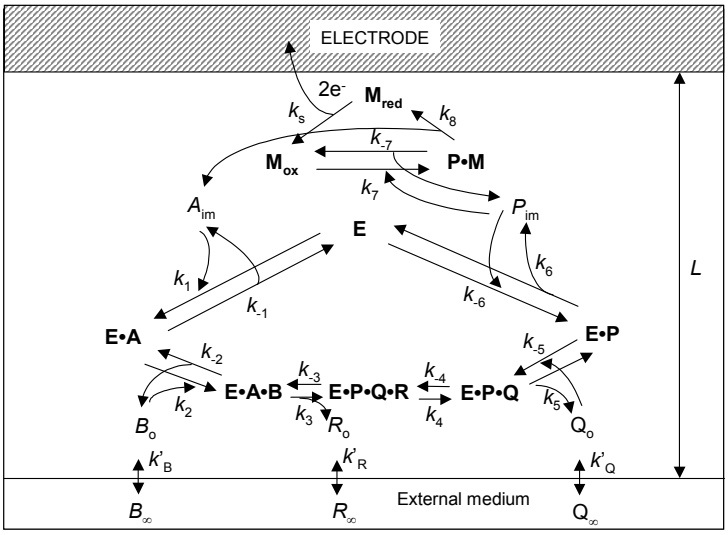

Figure S-4. Reaction scheme for a reagentless glutamate biosensor.

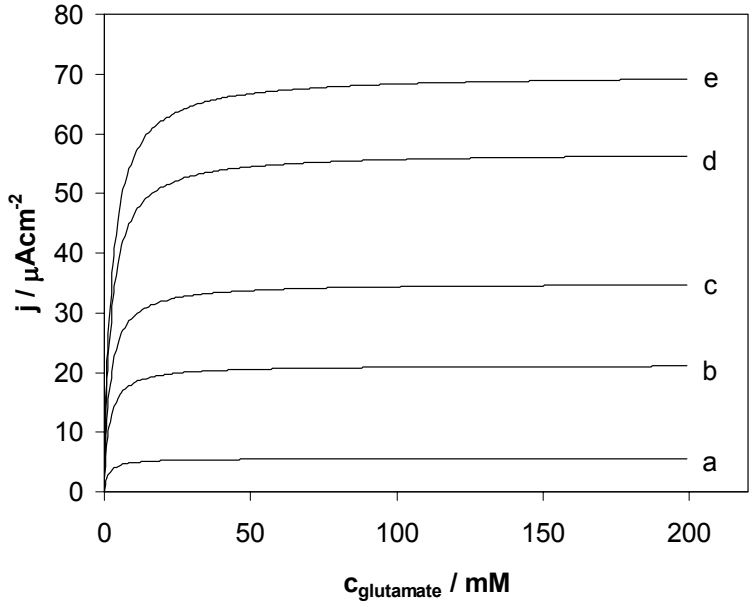

(A)

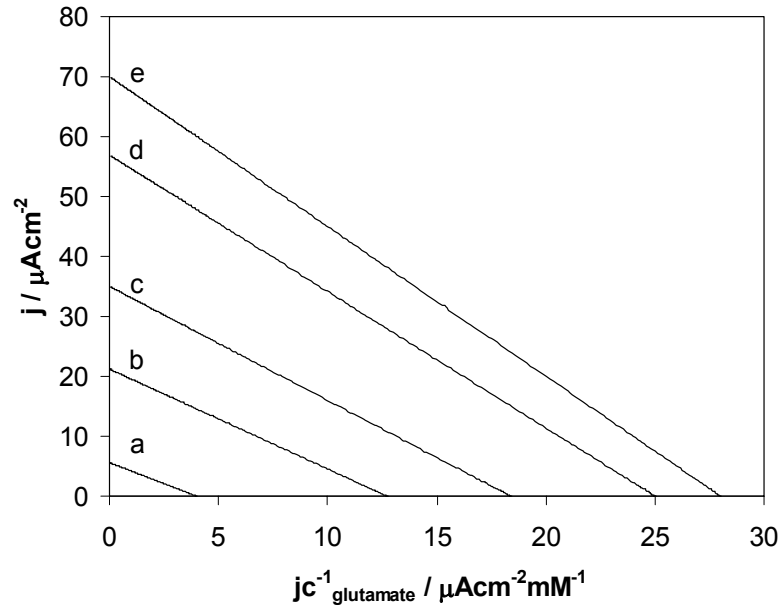

(B)

Figure S-5. Simulation of calibration curves **(A)** and Eadie-Hofstee plots **(B)** for the reagentless glutamate biosensors with varying loading of NAD^+ in the hydrogel (A_t): a) 0.02 mM ; b) 0.1 mM; c) 0.23 mM; d) 1 mM; e) ∞. The values of other parameters are: $\Gamma k_{cat} \rightarrow \infty$; $k'_B \rightarrow \infty$; $k'_Q \rightarrow \infty$; $k'_R \rightarrow \infty$; $LV_1 = 3.63\text{x}10^{-10}$ mol s^{-1} cm^{-2}; K_M = 0.8 mM; K_A = 0.23 mM; K_B = 2.5 mM; K_{AB} = 0.3 mM^2; K_{iA} = 10 mM; K_{iB} = 11 mM; K_R = 20 mM; K_Q = 0.25 mM; K_P = 0.04 mM; K_{iR} = 9 mM; K_{iQ} = 1.6 mM; K_{iP} = 0.03 mM.

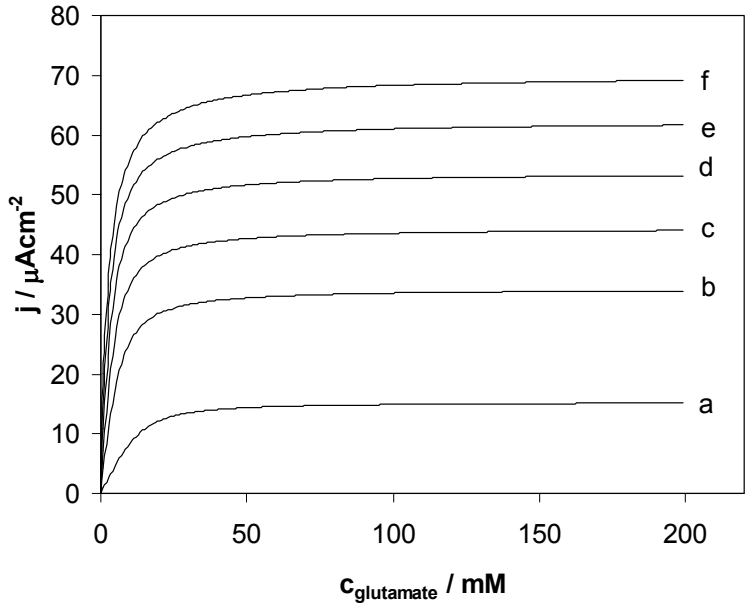

(A)

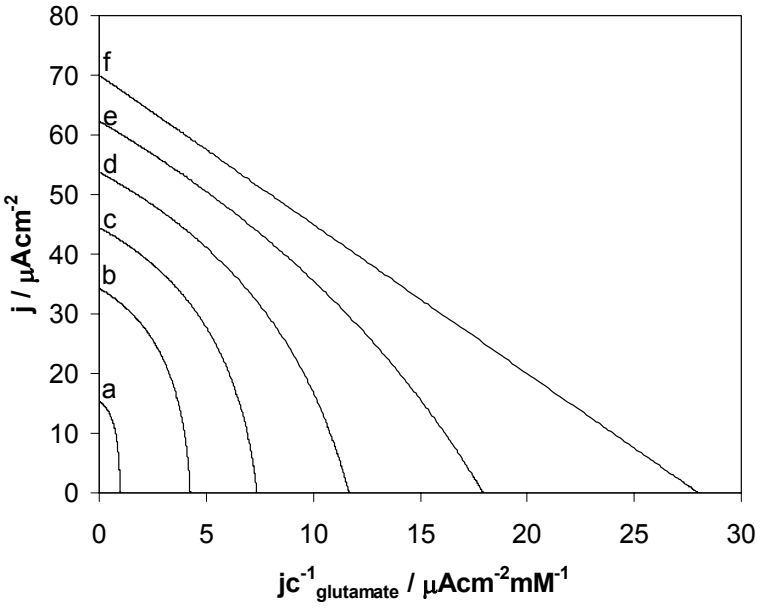

(B)

Figure S-6. Simulation of calibration curves **(A)** and Eadie-Hofstee plots **(B)** for the reagentless glutamate biosensors at $\Gamma k_{cat} \rightarrow \infty$ with varying mass transfer coefficients (k'_B, k'_Q, k'_R): a) 5.18×10^{-12} cm s^{-1}; b) 2.6×10^{-11} cm s^{-1}; c) 5.18×10^{-11} cm s^{-1}; d) 1.03×10^{-10} cm s^{-1}; e) 2.6×10^{-10} cm s^{-1}; f) ∞. The values of other parameters are: $A_t \rightarrow \infty$; $LV_1 = 3.63 \times 10^{-10}$ mol s^{-1} cm^{-2}; $K_M = 0.8$ mM; $K_A = 0.23$ mM; $K_B = 2.5$ mM; $K_{AB} = 0.3$ mM^2; $K_{iA} = 10$ mM; $K_{iB} = 11$ mM; $K_R = 20$ mM; $K_Q = 0.25$ mM; $K_P = 0.04$ mM; $K_{iR} = 9$ mM; $K_{iQ} = 1.6$ mM; $K_{iP} = 0.03$ mM.

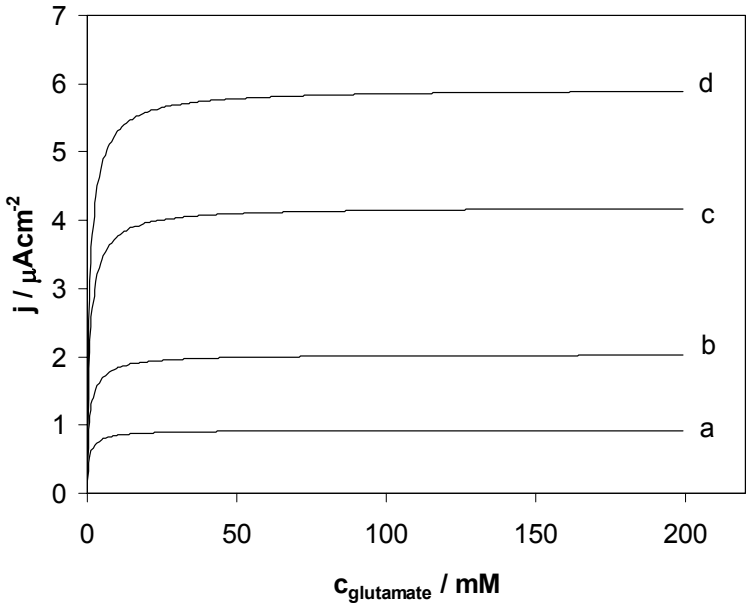

(A)

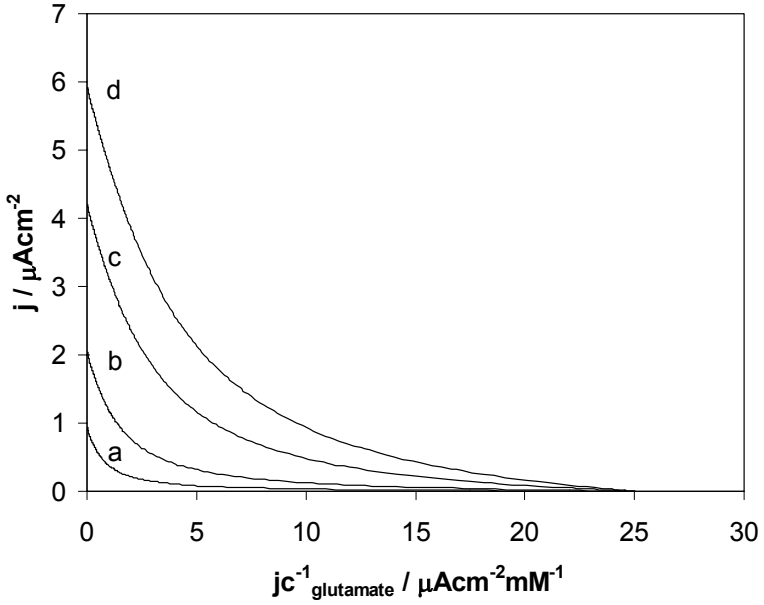

(B)

Figure S-7. Simulation of calibration curves **(A)** and Eadie-Hofstee plots **(B)** for the reagentless glutamate biosensors with varying maximum fluxes of the electrochemical NADH oxidation (Γk_{cat}): a) 2.6×10^{-11} mol s^{-1} cm^{-2}; b) 1.04×10^{-10} mol s^{-1} cm^{-2}; c) 4.15×10^{-10} mol s^{-1} cm^{-2}; d) 8.3×10^{-10} mol s^{-1} cm^{-2}; e) 1.7×10^{-9} mol s^{-1} cm^{-2}; f) 1.3×10^{-8} mol s^{-1} cm^{-2}; g) 5.178×10^{-8} mol s^{-1} cm^{-2}; h) ∞. The values of other parameters are: A_t=1 mM; $k'_B \rightarrow \infty$; $k'_Q \rightarrow \infty$; $k'_R \rightarrow \infty$; LV_l=3.63×10^{-10} mol s^{-1} cm^{-2}; K_M = 0.8 mM; K_A = 0.23 mM; K_B = 2.5 mM; K_{AB} = 0.3 mM^2; K_{iA} = 10 mM; K_{iB} = 11 mM; K_R = 20 mM; K_Q = 0.25 mM; K_P = 0.04 mM; K_{iR} = 9 mM; K_{iQ} = 1.6 mM; K_{iP} = 0.03 mM.

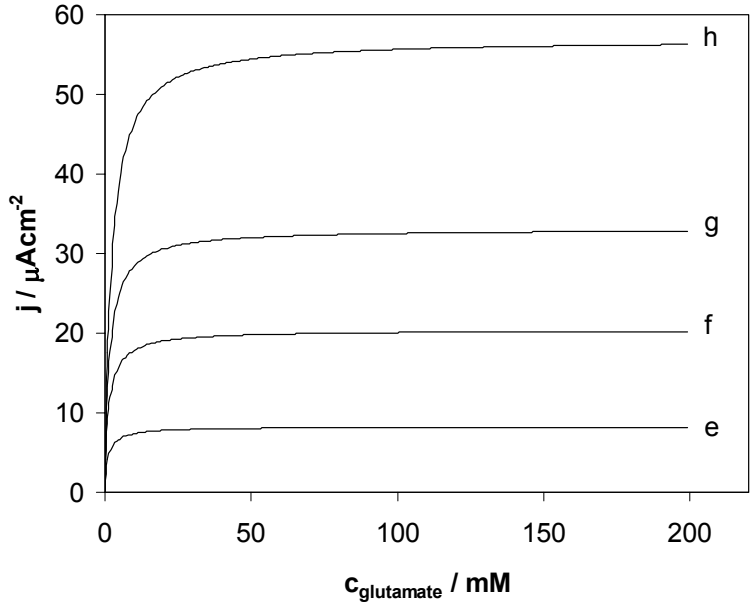

(A)

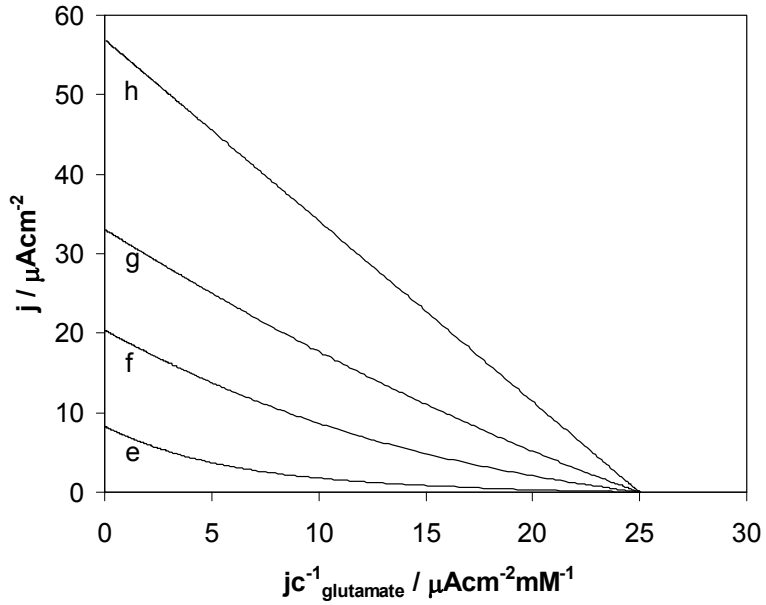

(B)

Figure S-7. (continued)

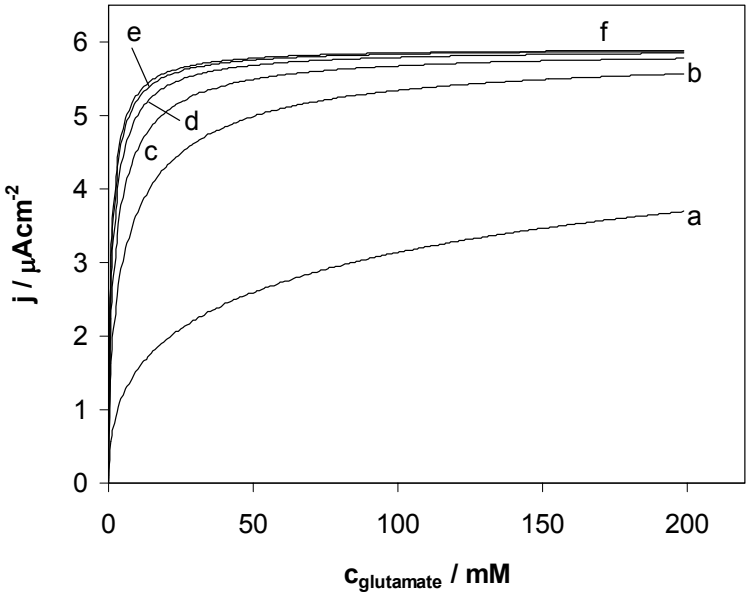

(A)

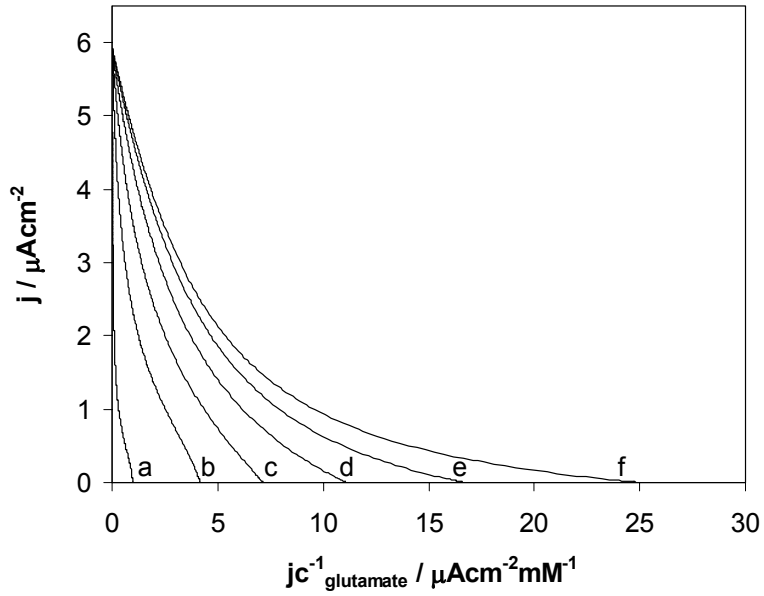

(B)

Figure S-8. Simulation of calibration curves **(A)** and Eadie-Hofstee plots **(B)** for the reagentless glutamate biosensors at Γk_{cat} equal to $8.3\text{x}10^{-10}$ mol s^{-1} cm^{-2} with varying mass transfer coefficients (k'_B, k'_Q, k'_R): a) $5.18\text{x}10^{-12}$ cm s^{-1}; b) $2.6\text{x}10^{-11}$ cm s^{-1}; c) $5.18\text{x}10^{-11}$ cm s^{-1}; d) $1.03\text{x}10^{-10}$ cm s^{-1}; e) $2.6\text{x}10^{-10}$ cm s^{-1}; f) ∞. The values of other parameters are: A_t=1 mM; $LV_1 = 3.63\text{x}10^{-10}$ mol s^{-1} cm^{-2};; K_M = 0.8 mM; K_A = 0.23 mM; K_B = 2.5 mM; K_{AB} = 0.3 mM^2; K_{iA} = 10 mM; K_{iB} = 11 mM; K_R = 20 mM; K_Q = 0.25 mM; K_P = 0.04 mM; K_{iR} = 9 mM; K_{iQ} = 1.6 mM; K_{iP} = 0.03 mM.

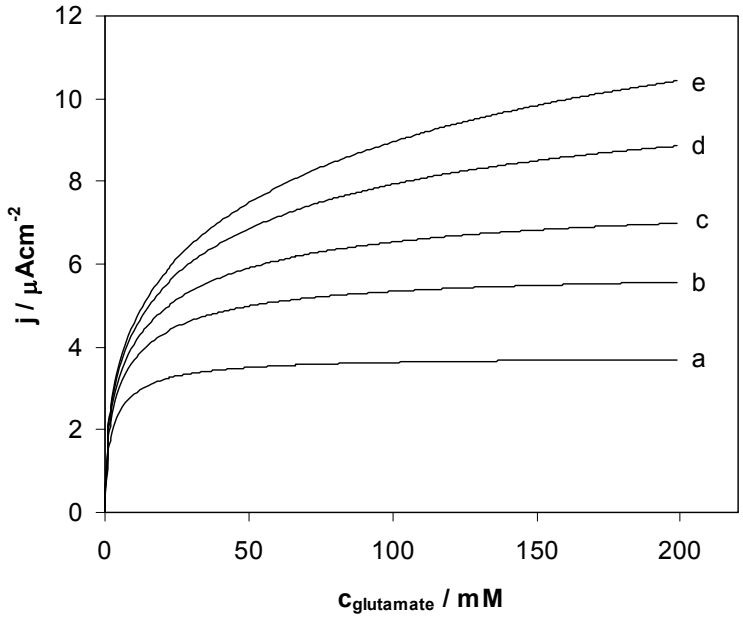

(A)

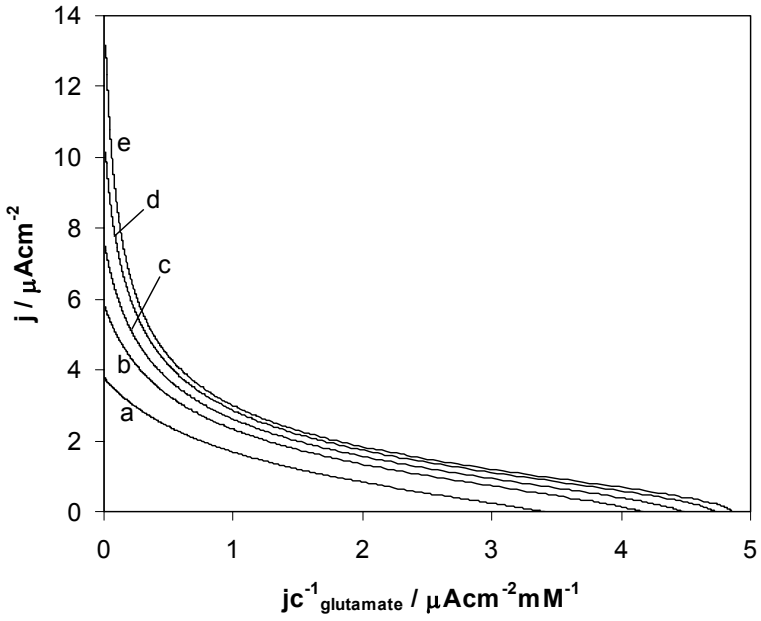

(B)

Figure S-9. Simulation of calibration curves **(A)** and Eadie-Hofstee plots **(B)** for the reagentless glutamate biosensors with varying maximum flux of enzymatic reduction of NAD^+ (LV_1): a) 1.55×10^{-10} mol s^{-1} cm^{-2}; b) 3.63×10^{-10} mol s^{-1} cm^{-2}; c) 6.22×10^{-10} mol s^{-1} cm^{-2}; d) 1.24×10^{-9} mol s^{-1} cm^{-2}; e) 2.49×10^{-9} mol s^{-1} cm^{-2}. The values of other parameters are: k'_B =2.6×10^{-11} cm s^{-1}; k'_Q =2.6×10^{-11} cm s^{-1}; k'_R =2.6×10^{-11} cm s^{-1}; A_t=1 mM; Γk_{cat} = 8.3×10^{-10} mol s^{-1} cm^{-2}; K_M = 0.8 mM; K_A = 0.23 mM; K_B = 2.5 mM; K_{AB} = 0.3 mM^2; K_{iA} = 10 mM; K_{iB} = 11 mM; K_R = 20 mM; K_Q = 0.25 mM; K_P = 0.04 mM; K_{iR} = 9 mM; K_{iQ} = 1.6 mM; K_{iP} = 0.03 mM.

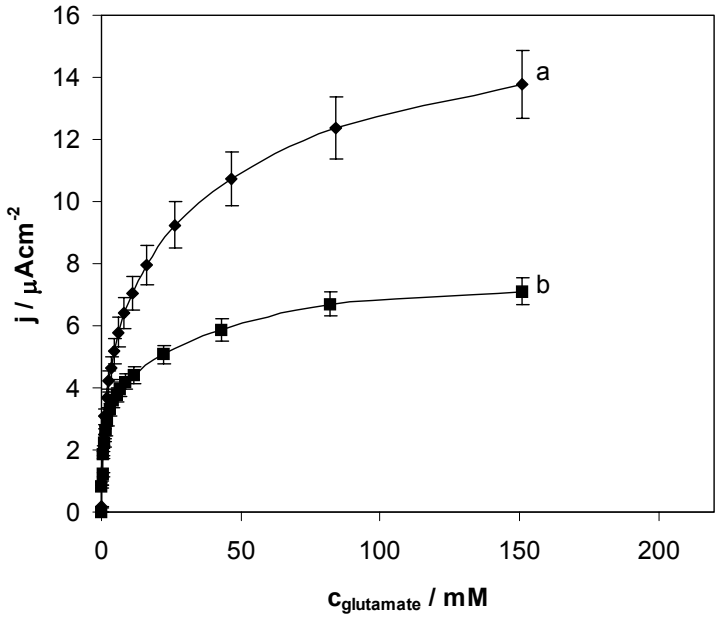

(A)

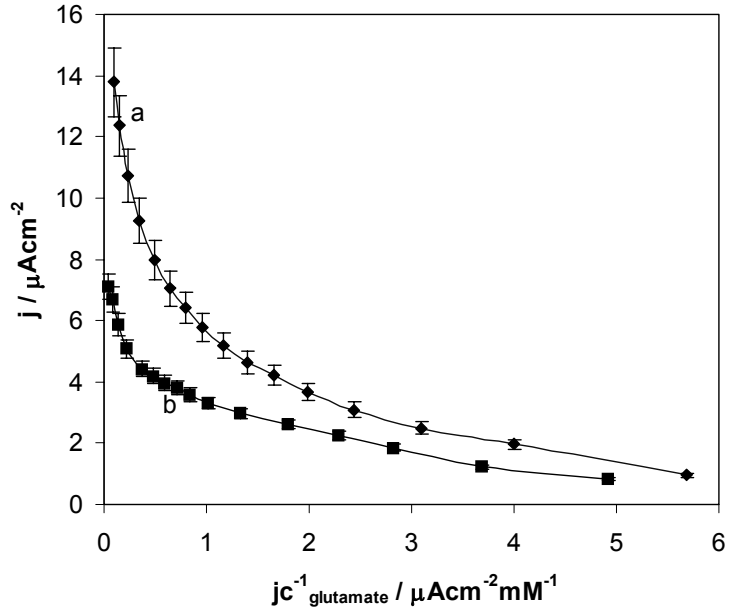

(B)

Figure S-10. Dependence of the apparent current density on L-glutamate concentration **(A)** and Eadie-Hofstee plots **(B)** for reagentless biosensors fabricated with the use of mesophilic GLDH based on: a) NAD^+-alginate; b) binder polymer. Experimental conditions: E_{app} 150 mV *vs*. Ag/AgCl,/KCl_{sat}, 0.1 M phosphate buffer (pH 7.4), temperature 30°C.

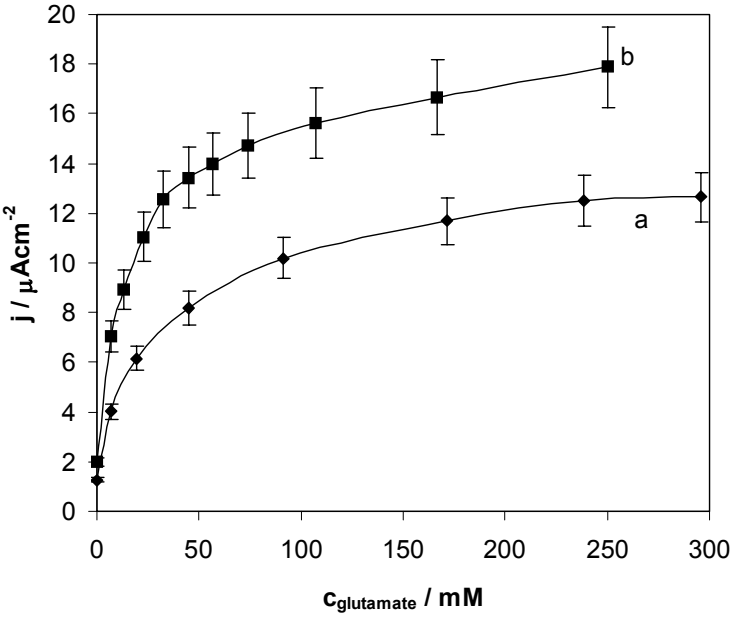

(A)

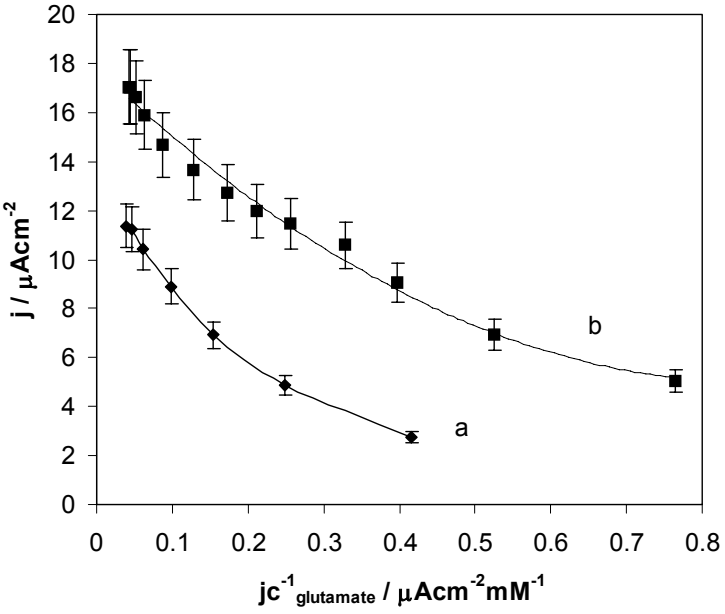

(B)

Figure S-11. Dependence of the apparent current density on L-glutamate concentration **(A)** and Eadie-Hofstee plots **(B)** for reagentless biosensors fabricated with the use of thermophilic GLDH based on: a) NAD^+-alginate; b) binder polymer. Experimental conditions: E_{app} 150 mV *vs.* Ag/AgCl/KCl_{sat}, 0.1 M phosphate buffer (pH 7.4), temperature 40°C.

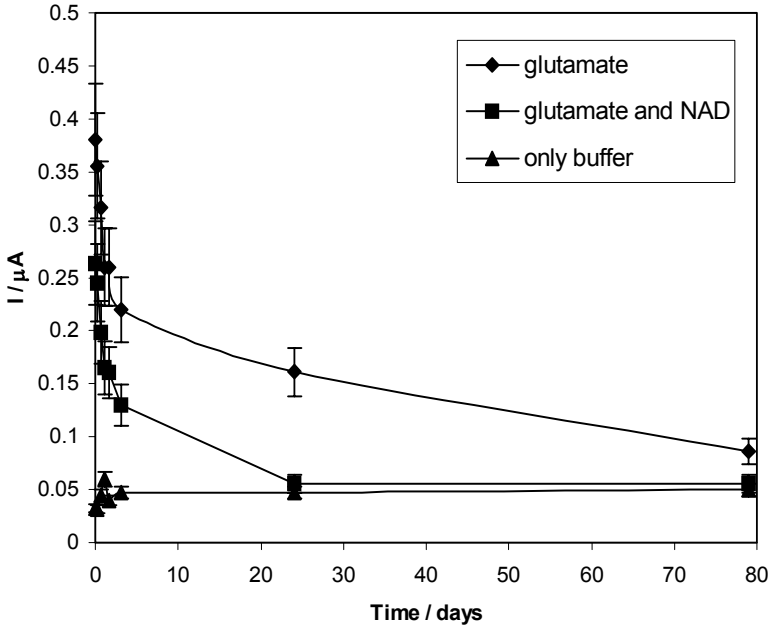

(A)

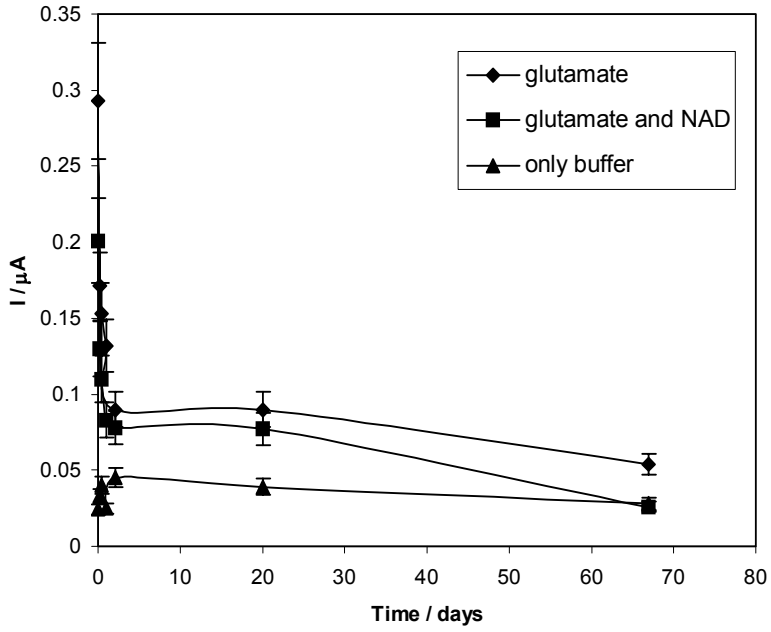

(B)

Figure S-12. Dependence of response current to 0.6 M glutamate, 0.6 M glutamate containing 0.18 M of NAD^+, and buffer on time obtained in shelf life study for the biosensors based on thermophilic **(A)** and mesophilic **(B)** GLDH

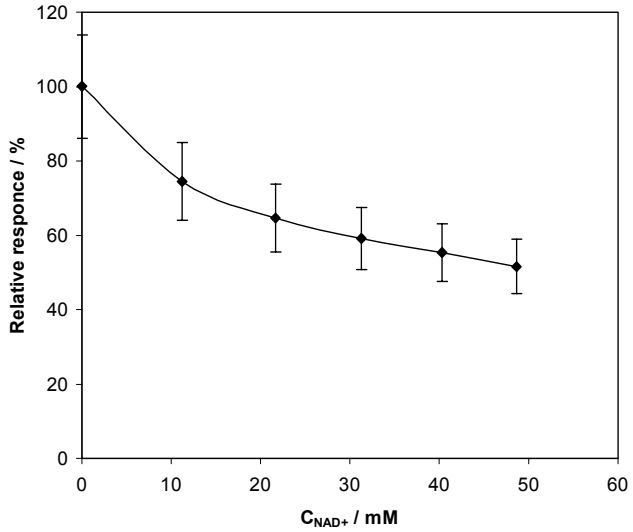

Figure S-13. Effect of NAD^+ on the response of graphite electrode in steady-state modified with osmium complex [Os(4,4'-dimethyl-2,2'-bipyridine)$_2$(1,10-phenanthroline-5,6-dione)]$(PF_6)_2$. Experimental conditions: surface coverage (2.3±0.2)x10^{-10}mol/cm^2, stirred 1.3 mM NADH solution in 0.1 M phosphate buffer deaerated with argon, pH 7.0, applied potential 150 mV *vs.* Ag/AgCl/KCl_{sat}.

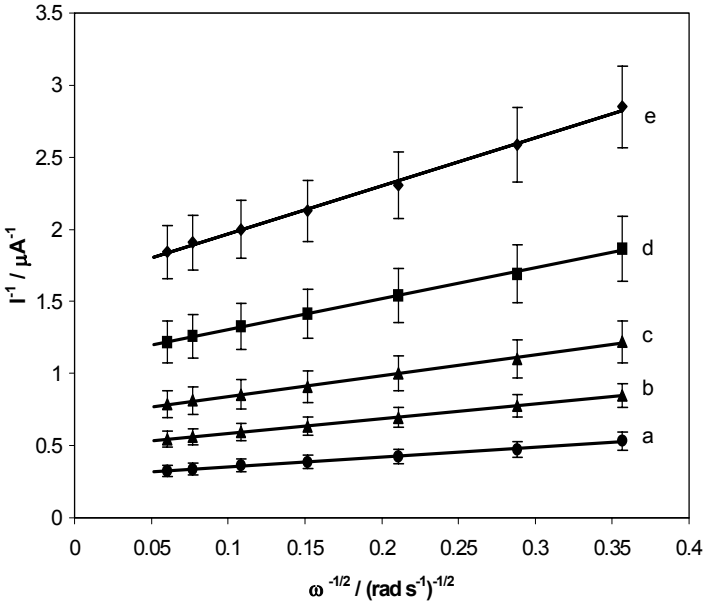

Figure S-14. Koutecky-Levich plot of steady-state electrocatalytic response for graphite RDE modified with [Os(4,4'-dimethyl-2,2'-bipyridine)$_2$(1,10-phenanthroline-5,6-dione)]$(PF_6)_2$ in the presence of 20 mM NAD^+ at different NADH concentrations: (a) 1.8 mM; (b) 1.2 mM; (c) 0.8 mM; (d) 0.533 mM; (e) 0.355 mM. Experimental conditions: surface coverage (2.8±0.3)x10^{-10}mol/cm^2, applied potential 200 mV *vs.* Ag/AgCl/KCl_{sat}, 0.1 M phosphate buffer deaerated with argon, pH 7.0.